Formation and stability of fibers obtained by cold gelation of pea protein isolate aggregates in a hydrodynamic spinning process

Alice Vilotte, Hugues Bodiguel, Deniz Gunes, Christophe Schmitt, Denis Roux, Emilie Guilbert, William Chèvremont, Clément de Loubens

Formation and stability of fibers obtained by cold gelation of pea protein isolate aggregates in a hydrodynamic spinning process

Alice Vilotte[a], Hugues Bodiguel[a,*], Deniz Z. Gunes[b,c], Christophe Schmitt[b], Denis Roux[a], Emilie Guilbert[a], William Chèvremont[d], Clément de Loubens[a]

[a] *Univ. Grenoble Alpes, CNRS, Grenoble INP, LRP, 38000 Grenoble, France*
[b] *Nestlé Research, Nestlé Institute of Food Sciences, Vers-Chez-Les-Blanc, Lausanne 26, CH-1000, Switzerland*
[c] *Current adress: Department of Chemical Engineering and Center for Food and Microbial Technology, KU Leuven, 3001 Leuven, Belgium*
[d] *ESRF, The European Synchrotron, CS 40220, Grenoble F-38043, France*

Abstract

Using plant protein sources in the formulation of food products is an important option to reduce the overall carbon footprint of the human diet. However, the ability to convert plant proteins into functional ingredients can hamper their use by the food industry. Our objective was to assemble pea protein isolate (PPI) aggregates into edible fibers. They were obtained by co-injection of a suspension of PPI aggregates with a solution of calcium chloride by means of physico-chemical bonds, i.e. in the absence of thermal treatment or chemical reaction. As soon as specific hydrodynamic conditions were met, homogeneous fibers of few hundreds μm diameter and few cm length were obtained. Small angle X-ray scattering showed that the building blocks of these fibers were dense aggregates of 400 nm radius. Calcium and PPI concentrations required for the processing of fibers were roughly given by the sol-gel state diagram of PPI aggregates. Compared to their dairy protein based equivalent, PPI fibers were obtained with a low mass fraction of protein (3% w/w) and were stable regardless of the concentration of calcium chloride used. We concluded that the robustness of the hydrodynamic spinning process was attributed to the strong reactivity of PPI aggregates with calcium ions and the low tendency of PPI gels to syneresis.

Keywords:
plant protein, gelation, SAXS, calcium, microstructure

1. Introduction

A wider use of plant protein sources in our diet is crucial to improve and re-balance the sustainability of the current food system. Fortunately, recent advances in crop selection, agricultural efficiency as well as the development of mild protein extraction processes have enabled a variety of plant protein ingredients for food formulation (Sim et al., 2021). Besides their nutritional value, these plant proteins have been shown to have multiple uses and functionalities in food applications, provided that they are properly chosen and combined with the other food ingredients in complex matrices (Kumar et al., 2022). Hence, it has been shown that due to the various extraction processes, plant proteins do exist in various colloidal states. It is therefore important to apply appropriate treatment to standardize and maximize their functionality during food formulation by controlling their aggregation state (Amagliani & Schmitt, 2017; Schmitt et al., 2021).

An interesting type of protein aggregate is micro or nano fiber, which allows production of various types of edible structures and textures (Kouhi et al., 2020). Protein fibrils of about 100 nm persistance length can be obtained by self-assembly of partially hydrolyzed proteins upon prolonged heat treatment in very acidic environment. It was initially applied to whey proteins, but was successfully tested on a variety of plant protein sources (Cao & Mezzenga, 2019; Li et al., 2023). The main limitation of this process is the time required for protein treatment as well as the harsh pH conditions, i.e. pH 2.0, which are difficult to scale up. Therefore, it is worthwile to look for alternative options to produce plant protein fibers.

Recently, long microscopic protein fibers ($\simeq$ 100 μm diameter) were obtained by a simple hydrodynamic method. The process consisted of co-injecting a suspension of whey protein isolate (WPI) fractal aggregates with a solution of calcium chloride (Vilotte et al., 2022). The sol-gel transition was triggered by the diffusion of calcium ions into the jet of aggregates. Gelation resulted from both screening of electrostatic interactions and specific binding of calcium ions with aggregated proteins (Alting et al., 2003; Kharlamova et al., 2018). Whereas fiber diameter was tuned by the hydrodynamic conditions, such conditions could also lead to hydrodynamic instabilities which limited the formation of the fibers. More importantly, strong non-monotonic effects of calcium concentration were reported due to a competition between micro-phase separation and osmotic phenomena which controlled the stability of the fibers.

Interestingly, pea protein isolate (PPI) was shown to have the ability to form aggregates upon heat treatment in order to produce nanoparticles or larger micrometer scale dense aggre-

*hugues.bodiguel@univ-grenoble-alpes.fr

gates (Tanger et al., 2021), while being sensitive to the presence of calcium ions (Fan et al., 2020; Amagliani et al., 2023).

The objective of this paper was to extend the process of hydrodynamic spinning of edible protein aggregates to PPI aggregates. They were obtained by heat-induced aggregation and co-injected with a solution of calcium chloride in a core-annular flow. The structure of PPI aggregates was investigated by small angle X-ray scattering (SAXS). Then, we studied the stability of these fibers, their microstructure and the range of hydrodynamic conditions leading to the formation of stable fibres. In this paper, we compare the results obtained with WPI (Vilotte et al., 2022) to new results obtained with PPI. As PPI aggregates have a higher reactivity to calcium ions than WPI aggregates (Silva et al., 2018), we expected to reveal some remarkable features of PPI based fibers.

2. Materials and methods

2.1. Suspensions of PPI aggregates

Pea protein isolate (PPI) Pisane C9 (batch 873053) was manufactured by Cosucra (Warcoing, Belgium). The proximal composition of the PPI was (in g/100g powder wet basis): protein 80.72, ash 5.37, moisture 4.15, fat 8.76. Protein composition was about 70% salt-soluble globulins and 5% water-soluble albumins (Moll et al., 2022).

A PPI solution of 5 % w/w was dissolved in demineralized water, 0.02 % w/w sodium azide was added to the solution to prevent bacterial growth. The solution was gently stirred for 3 h at ambient temperature until complete dissolution of PPI powder and then homogenized at 250 bars with a two-stage high pressure homogenizer PandaPLUS 2000 (GEA) to ensure maximum solubility of the pea protein (Moll et al., 2021; Amagliani et al., 2023). The pH was adjusted at 7.0 with 1M HCl.

Solutions of calcium chloride were prepared by dissolving $CaCl_2$,$2H_20$ powder purchased from Sigma-Aldrich (CAS number 10035-04-8) into demineralized water. The concentration of calcium chloride $C_{Ca^{2+}}$ ranged from 35 mM and 5.9 M.

PPI aggregates were produced by heating the solution of 5% w/w PPI for 15 min at 95°C in 10 mL Pyrex tubes. The suspension of aggregates was then cooled down in an ice bath and kept at 4°C during one night. The hydrodynamic radius R_h of the aggregate was measured by Dynamic Light Scattering (VASCO Particle size Analyzer, Cordouan Tech.) and was about 400 nm. Figure 1-b shows the sol-gel state diagram of PPI aggregates. We also reported results obtained with WPI aggregates, see Vilotte et al. (2022) for details. Briefly, the suspension of fractal WPI aggregates was obtained by heating a solution of 8 % w/w WPI at 10 mM NaCl and pH 7.0 at 92°C for 30 min. The aggregates had a 70 nm R_h and fractal dimension of 2 (Vilotte et al., 2021). The sol-gel state diagram of WPI aggregates has been studied by Kharlamova et al. (2018) .

In order to keep the size of the aggregates constant over the whole study, the concentration of the suspensions of PPI and WPI aggregates, C_{agg}, was varied by dilution or by gentle evaporation at 30°C for several hours under stirring.

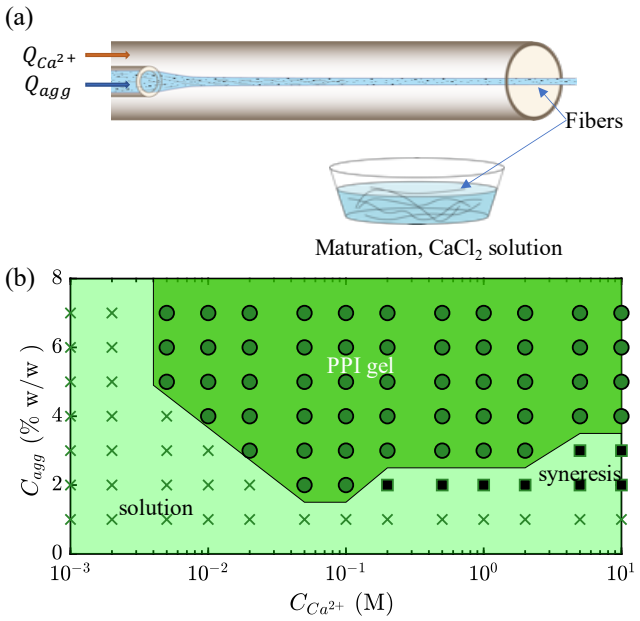

Figure 1: **a:** Fibers were obtained by co-injecting a suspension of PPI aggregates with a suspension of calcium chloride. The residence time was fixed at 6 s, whatever the flow rates used. Fibers were then stored in a calcium bath for 20 min (maturation step) to complete their gelation. **b:** State diagram of PPI gelation and syneresis. PPI aggregates were obtained by heating 5 % w/w PPI, pH 7.0 at 95°C for 15 min.

2.2. Small-Angle X-Ray Scattering

The structure of PPI and WPI aggregates was characterized by SAXS experiments (Echaniz et al., 2025) on beamline ID02, ESRF (Grenoble) which offered an energy of 8.0 - 20.0 keV and a sample-detector distance from 1.5 m to 31 m (Narayanan et al., 2018). We perform measurements at 10 m and 31 m at fixed energy of 12.230 keV, which correspond to a range of scattering vector (q) from 2×10^{-3} to 0.3 nm^{-1}. Samples were analyzed under static conditions in a flow through quartz capillary of 2 mm inner diameter. This made it possible to measure the background and the sample at the same specific point, which ensured a good background subtraction. The exposition time was set to 0.5 s. This value has been determined to get enough statistics for each spectrum, without any sample radiation damages seen on the scattering curves. In addition, the sample has been pushed forward into the capillary, so that a fresh sample is measured for each acquisition. For each sample, the background of the cell containing water and 10 spectra were acquired. Spectra of aggregates were obtained by averaging the 10 data sets and subtracting the background. For both suspensions of protein aggregates (i.e. 8 % w/w WPI, 10 mM NaCl, pH 7.0 at 92°C during 30 min and 5 % w/w PPI, pH 7.0 at 95°C during 15 min), the spectrum could be assimilated to the form factor of the aggregates, as the scattered intensity was linear with respect to the aggregate concentration, in the whole range of scattering vector (data not shown).

The radius of gyration R_g of the WPI and PPI aggregates was measured in the low q range ($q \ll 1/R_g$) of the scattered

intensity I using the Guinier analysis,

$$I(q) = I_0 \exp\left(-q^2 R_g^2/3\right) \quad (1)$$

where I_0 is the scattered intensity when q tens to 0. R_g was obtained by a least-square fitting.

2.3. Hydrodynamic spinning

Fibers were obtained by co-injecting the suspension of PPI aggregates with a solution of $CaCl_2$ in a coaxial needle (Ramé-Hart Instruments), with inner and outer radii r_i = 178 μm and r_o = 356 μm, respectively (Fig. 1). The needle was embedded into a fluorinated ethylene-propylene flexible tube (Fluigent) immersed in a water-bath (27°C). Core and annular flow rates, Q_{agg} and $Q_{\text{Ca}^{2+}}$, were controlled by a syringe pump (Nemesys, Cetoni). The residence time τ_r was kept fixed at 6 s by varying the tube length L from 11 to 225 cm. We defined the mean velocity by $v = (Q_{\text{agg}} + Q_{\text{Ca}^{2+}})/\pi r_0^2$ and τ_r by the ratio v/L. The diameter of the jet D of aggregates can be calculated by solving momentum balance and mass conservation equations in laminar flow conditions (Bonhomme et al., 2011). In the limit of low viscosity ratio $m = \eta_{Ca^{2+}}/\eta_{agg}$, it reads $D = 2r_0/\sqrt{1+2\alpha}$, where $\alpha = Q_{agg}/Q_{Ca^{2+}}$ is the ratio of flow rates, $\eta_{Ca^{2+}}$ and η_{agg} the viscosities of the solution of $CaCl_2$ and aggregates, respectively. In our study, v ranged from 10^{-2} to 0.8 m/s and q from 1 to 100. In these conditions, the Reynolds number Re= $\rho v r_0/\eta_{Ca^{2+}}$ ranged from 4 to 200. We showed in our previous paper the need to finely control hydrodynamic parameters in order to obtain long WPI fibers (Vilotte et al., 2022). Further in this paper, we show that the same hydrodynamic considerations apply for the hydrodynamic spinning of long PPI fibers.

As the time scale of calcium diffusion through the jet of aggregates $\tau_d \simeq r_i^2/D_{Ca^{2+}}$ is of the order of 300-500 s, the residence time of 6 s was not sufficient to induce a full gelation of the jet. So, we collected the pre-formed fiber into a calcium bath (at the same concentration as the flux), in which they were stored for 20 min. Our previous experiments with dairy proteins showed that this step was very critical for the stability of the WPI fibers (Vilotte et al., 2022). In this paper, we investigate the stability conditions for the production of PPI fibers so to compare them with the WPI fibers

Lastly, parameters which were varied in this paper were C_{agg}, $C_{Ca^{2+}}$, L, v and α. The residence time in the tube and in the calcium bath was set to 6 s and 20 min, respectively.

2.4. Microscopy

Fibers were observed by bright field microscopy (Olympus IX-72) with a ×4 objective just after the production, and all along the maturation step.

The inner structure of the fibers was observed by scanning electron miscroscopy (SEM). First, fibers were washed with distilled water, freeze-dried and pasted on a stub covered with double-sided carbon tape. Then, the specimens were coated with Au/Pd and secondary electron images were recorded with an FEI Quanta 250 scanning electron microscope equipped with a field emission gun and operating at 2.5 kV.

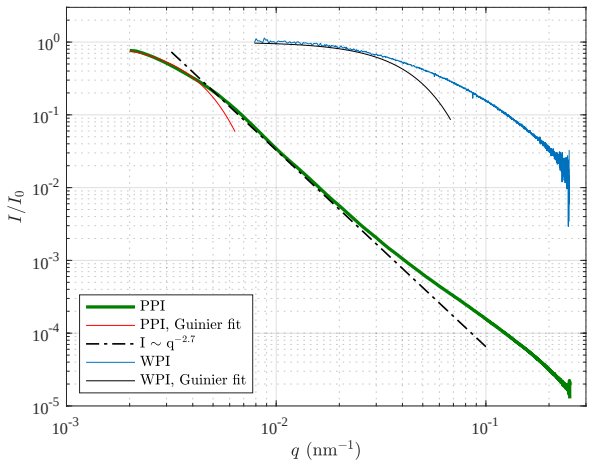

Figure 2: Normalized scattered intensity I/I_0 as a function of the scattering vector q for suspensions of PPI (green line, 5 % w/w PPI, pH 7.0 at 95°C for 15 min) and WPI (blue line, 8% w/w WPI, 10 mM NaCl, pH 7.0 at 92°C for 30 min) aggregates used to produce the fibers. Red and black lines are Guinier fits (Eq. 1) for PPI and WPI aggregates, respectively. The dashed black line is $I \sim q^{-2.7}$.

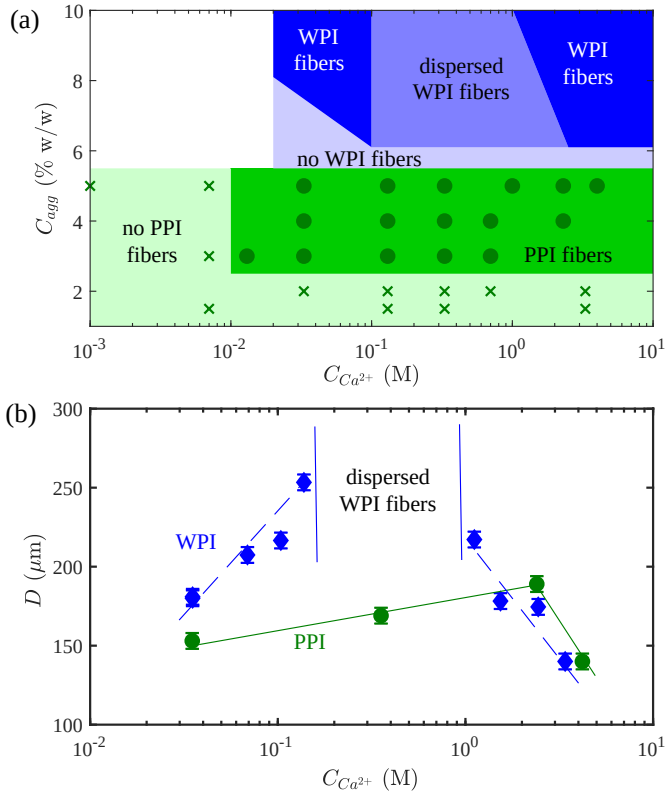

Figure 3: **a:** State diagram of PPI fiber formation and maturation. Green circles stand for stable PPI fibers within 20 min of maturation step. Green crosses are for cases where no PPI fibers were formed. The state diagram of PPI fiber formation is compared with that of the WPI obtained by Vilotte et al. (2022) for the same hydrodynamic conditions. v=7.4x10^{-2} m/s and α=10. **b:** Fiber diameter after 20 min maturation as a function of calcium concetration for 5% w/w PPI fibers (circles) and 10% w/w WPI fibers (diamonds).

3. Results and discussion

3.1. Structure of PPI aggregates

In this section, we analyse the structure of the PPI aggregates used to produce the fibers by co-injection of a suspension of PPI aggregates with a solution of calcium chloride at 27°C, Figure 1-a. Two steps were required to obtain the PPI aggregates. First, a dispersion of PPI was microfluidified to increase their solubility and decrease the particle size from 100 μm radius to 100 nm radius, see Moll et al. (2021) for details. Then, a 5% w/w PPI suspension at neutral pH was heated at 95°C for 15 min. Guinier analysis of static X-ray scattering intensity of the heated suspensions of PPI shows that the radius of gyration R_g of the aggregates was 460 nm, green line in Fig. 2. This value is in line with the hydrodynamic radius obtained by DLS (R_h = 400 nm), and laser diffraction analysis carried out by Amagliani et al. (2023). So, the heat treatment increased the size of the aggregates by a factor of 4.

Fitting $I(q)$ by a power law in the range 5.10^{-3} - 3.10^{-3} nm^{-1} shows that the fractal dimension d_f of PPI aggregates was about 2.7, which corresponds to a compact object and is significantly higher than the 2.0 reported for heated soy globulin (Chen et al., 2016). At high q (>0.09 nm^{-1}), an inflection is visible on the spectra. The Porod plot (Iq^4 as a function of q, data not shown) presents an oscillation in the high q range. This oscillation is characteristic of the scattering of a sphere. By fitting the scattering intensity of a suspension of (monodisperse) spheres on the data, a radius of about 10 nm was estimated.

All these results lead us to the conclusion that there are three important scales in the q range 10^{-3} - 0.2 nm^{-1}. The 400 nm aggregates obtained after the heating process were the result of the aggregation of some compact soluble aggregates obtained by microfluidization. These compact aggregates were themselves composed of 10 nm entities.

Contrary to PPI aggregates, it is well established that WPI aggregates obtained by heat-induced aggregation at pH 7.0 are characterized by a fractal dimension of about 2 and that their size can be tuned by the ionic strength (Gimel et al., 1994; Mehalebi et al., 2008; de Guibert et al., 2020; Vilotte et al., 2021). More specifically, WPI aggregates used to produce fibers in our previous publication (Vilotte et al., 2022) were 10 times smaller than PPI aggregates, R_g = 40 nm, blue line in Fig. 2. The hydrodynamic radius of WPI aggregates obtained by DLS was larger than R_g obtained by DLS, R_h = 70 nm. The polydispersity, the porous structure and the weak scale separation between WPI aggregates and the oligomers could explain this difference.

3.2. Fiber stability during the maturation step

The role of physicochemical parameters on the formation and stability of PPI fibers was first studied by varying the PPI concentration C_{agg} and calcium concentration $C_{Ca^{2+}}$ during the hydrodynamic process and the maturation step. The hydrodynamic parameters were chosen far from the stability limits of the jet, i.e. v = 7.4 10^{-2} m/s and q = 10, see below.

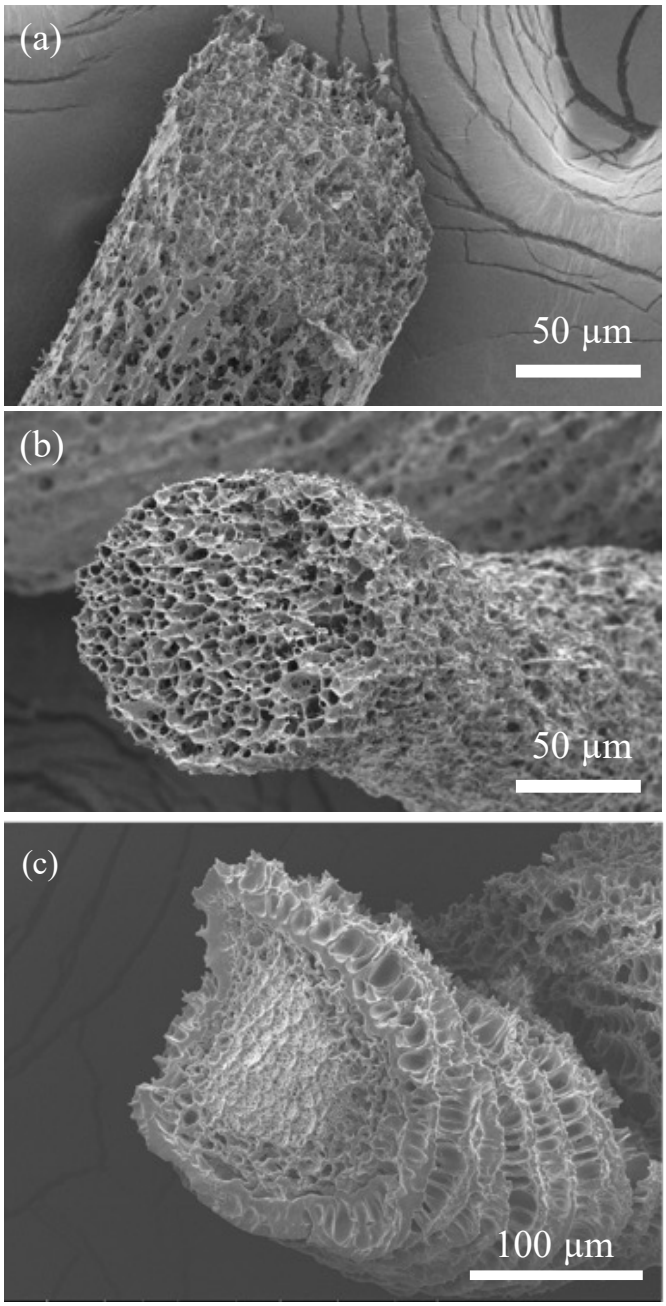

Figure 4: Scanning electron microscopy images of 5% w/w PPI fibers obtained with **(a)** 35 mM and **(b)** 4 M calcium chloride. **(c)** Scanning electron microscopy images of 8% w/w WPI fibers obtained with 2.9 M calcium chloride, adapted from Vilotte et al. (2022).

The state diagram of the formation of PPI fibers shows two regions: either PPI fibres were formed and remained stable during the maturation step, or no fibres were formed, green areas in Fig. 3-a. PPI fibers could not be obtained if C_{agg} was lower than 2.5 % w/w and $C_{Ca^{2+}}$ was lower than 0.01 M. These limits corresponded roughly to the limits of sol-gel transition as shown in the state diagram in Fig. 1-b. The sol-gel phase diagram shows a small domain at high $C_{Ca^{2+}}$ and low C_{agg} characterized by syneresis (black squares), which did not seem to limit the formation of fibers.

This state diagram was surprisingly simple in comparison with that of WPI fibers (Vilotte et al., 2022), which is summed up in blue in Fig. 3-a. As for PPI fibers, WPI fibers were obtained only if C_{agg} was larger than a threshold of 6% w/w instead of 2.5% w/w for PPI aggregates. This difference highlights that PPI aggregates can be more easily cross-linked by calcium ions than WPI aggregates, which is explained by a higher affinity between PPI and calcium ions (Silva et al., 2018). Moreover, WPI fibers produced between 0.2 and ≃2 M $CaCl_2$ swelled and dispersed during the maturation step. Above ≃2 M $CaCl_2$, stable fibers were again obtained. Dispersion of WPI fibers was concurrent with the emergence of syneresis in the sol-gel state diagram of WPI aggregates which starts for $C_{Ca^{2+}}$ as small as .01 M; see Kharlamova et al. (2018) for details. This limit was ten times higher for PPI aggregates, which explains why the dispersion of PPI fibers was not observed. But a closer look of the evolution of the diameter D of the fibers with $C_{Ca^{2+}}$ showed that PPI fibers also swelled up to 3 M $CaCl_2$, Fig. 3-b. In contrast to WPI fibers, the increase in diameter was limited and did not lead to dispersion of the fibers. This is fully consistent with the difference in the syneresis limit value between the two systems. Above 3 M, the diameter of PPI fibers decreased. We observed the same phenomenon for WPI fibers. This shrinking was interpreted as the consequence of an osmotic phenomenon triggered by the high difference of chemical potential between the suspensions of aggregates and the solution of $CaCl_2$ at high concentration (Vilotte et al., 2022). This osmotic pressure difference creates a flux of water from the fiber towards the calcium which concentrates the aggregate in the fiber and promotes a sol-gel transition.

To summarize, PPI aggregates present several remarkable features of the process of their shaping into fibers. Compared to WPI aggregates, their greater reactivity with calcium ions allowed us to produce fibres with a smaller concentration of PPI than of WPI. In addition, syneresis phenomena were strongly delayed during the ionic gelation of PPI aggregates, which allowed PPI fibers to remain stable, regardless of the calcium chloride concentration used.

3.3. Fiber structure

For PPI fiber as wall, the decrease in diameter at high calcium concentration was attributed to the existence of an osmotic flux that shrunk the fibers. This phenomenon is due to a small selectivity of the gels to calcium chloride and will be described in detail in a forthcoming paper. The first consequence of this phenomenon is the shrinkage of the object, as reported in Fig. 3-b for WPI and PPI fibers at high calcium concentration. In the case of WPI fibers, a second consequence was observed: the spontaneous formation of a core-shell structure due to the transport of aggregates by the osmotic flux and their concentration in the shell. SEM images of PPI fibers at low and high calcium concentration (Fig. 4-a, b) do not show any evidence of a denser shell, conversely to WPI fibers (Fig. 4-c) . Note that the apparent porosity seen o the SEM images was due to the freeze-drying process applied prior to performing SEM examination. The formation of a core-shell structure is influenced by various parameters, including the permeability of the gel, its selectivity towards calcium ions, and the reaction rate. In the case of PPI aggregates, based on our observations, we can only speculate that the necessary combination of physicochemical conditions required for the formation of core-shell fibers was not achieved.

3.4. Hydrodynamic conditions for the spinning of aggregates

Lastly, the influence of hydrodynamic parameters on the formation of PPI was briefly studied and compared with our extensive study on WPI fibers (Vilotte et al., 2022). Fig. 5-a shows the state diagram of PPI fiber formation (green) in the v-α plane. Blue dashed lines are the two limits of stability as observed for WPI fibers, noted $v_1(\alpha)$ and $v_2(\alpha)$. The state-diagram is also illustrated by pictures of WPI and PPI fibers at fixed outlet velocity $v = 7.4\ 10^{-2}$ m/s and various flow rate ratios α, Fig. 5-c. As for WPI fibers, long PPI fibers were obtained in a well-defined window of hydrodynamic parameters. At high outlet velocity $v > v_2$, no or cut fibers were obtained. This limit was explained by inertia-driven instabilities in core-annular flow of miscible fluids Cubaud & Notaro (2014), see Vilotte et al. (2022) for details on WPI fibers. In short, the destabilization of the flow can be triggered either by diffusion or inertia, depending on the values of the Péclet (Pe) and Reynolds (Re) numbers (Cubaud & Notaro, 2014). In our experiments, the flow conditions were stable concerning diffusive instabilities as $\mathrm{Pe} = v r_o / D_{Ca^{2+}}$ was larger than the threshold value of 0.5×10^4 reported by Cubaud & Notaro (2014). Inertia destabilizes also miscible core-annular flow if the Reynolds number is larger than $900/\alpha$ for a viscosity ratio of 10 (Cubaud & Notaro, 2014). This order of magnitude was roughly in line with the v_2 limit obtained for WPI fibers. Note that the limit was slightly larger for PPI than for WPI fibers, which could be due to differences in the kinetics of gelation. At low v and high α ($< v_1$), pieces of gel were obtained instead of long fibers. We observed that a clog was formed at the outlet of the inner nozzle and regularly evacuated. This limit is reached when the characteristic time of PPI gelation τ_g is equivalent to the residence time of the aggregates in the entrance region of the core-annular flow ($\simeq r_0$), i.e. $v_1(\alpha) = r_0(\alpha + 1)/\tau_g$. Consequently, we estimated a characteristic time of gelation for PPI aggregates of about 0.8 s.

One important feature of the spinning hydrodynamic process is the possibility of tuning the diameter of the fiber thanks to the flow rate ratio α. In fact, the diameter of the jet in core-annular flow is simply given by $D = 2r_0/\sqrt{1 + 2\alpha}$, in the limit of low viscosity ratio $m = \eta_{Ca^{2+}}/\eta_{agg}$. Consequently, the diameter of the fiber D could be tuned by α and roughly followed to this hydrodynamic law, Fig. 5-b,c. However, D was smaller for fibers obtained with high calcium concentration, which was consistent with the above-mentioned osmotic phenomena. It was also possible to obtain fibers on a larger range of α when the calcium concentration was increased.

4. Conclusion

In conclusion, we generalized the process of hydrodynamic spinning of protein aggregates to a plant protein, namely pea

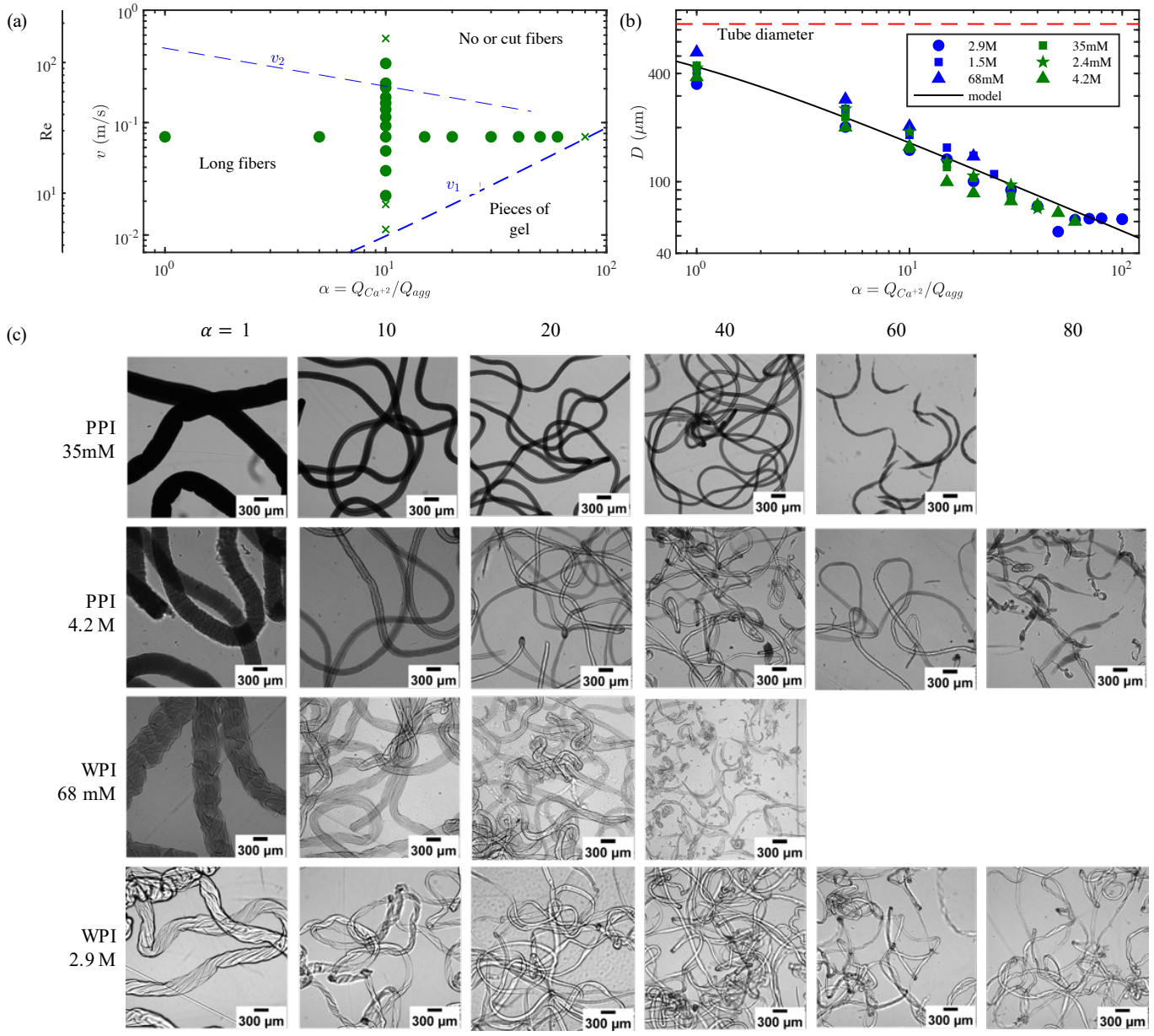

Figure 5: **a:** State diagram of PPI fiber production in the $v - \alpha$ plane for 5% w/w PPI and 4.2 M $CaCl_2$. Circles correspond to the formation of long PPI fibers, whereas crosses show the formation of pieces of gel or cut fibers. Blue dashed lines show the limit of stability for WPI fibers (8% w/w WPI and 1.5 M $CaCl_2$ from Vilotte et al., 2022). **b:** Fiber diameter measured just after the production, for $v = 7.4 \times 10^{-2}$ m/s as a function of the flow rate ratio α. Green and blue symbols correspond to 5% w/w PPI and 8% w/w WPI fibers for different $CaCl_2$ concentration. The solid line is the model prediction, $D = 2r_o\,(1 + 2q)^{-1/2}$. **c:** Images of fibers formed with PPI and WPI aggregates for different $CaCl_2$ concentration, v=7.4x10^{-2} m/s, t_{flow}=6 s.

protein isolate. Using this process, we produced long PPI protein fibers of few hundreds micrometer diameter. Static X-ray scattering showed that the basic bricks of these fibers were PPI aggregates of 400 nm radius and possess a characteristic dense structure at least above a 10 nm scale. The strong affinity of these aggregates to calcium ions allowed us to form fibers with a small mass fraction of PPI (3% w/w). Furthermore, while dairy protein gels were rapidly subject to syneresis, PPI gel was not, making PPI fibres very stable regardless of calcium concentration. Hence, we can infer that the hydrodynamic process was robust, provided that the hydrodynamic conditions are carefully selected to ensure stable formation of fibres. Finally, we concluded that the hydrodynamic spinning of PPI aggregates demonstrates the possibility of exploiting the colloidal interactions of plant proteins in food processes in order to develop new sustainable ingredients.

Declaration of competing interest

The authors declare that they have no known competing financial interests or personal relationships that could have appeared to influence the work reported in this paper.

CRediT authorship contribution statement

Alice Vilotte: Conceptualization, Investigation, Writing - original draft. Hugues Bodiguel: Conceptualization, Investigation, Supervision, Writing - original draft. Deniz Z. Gunes: Conceptualization, Supervision, Writing - review & editing. Christophe Schmitt: Conceptualization, Supervision, Writing - review & editing. Denis Roux: Investigation, Supervision, Writing - review & editing. Emilie Guilbert: Investigation, Writing - review & editing. William Chèvremont: Investigation, Writing - review & editing. Clément de Loubens: Conceptualization, Investigation, Supervision, Writing - original draft.

Acknowledgements

LRP is part of the LabEx Tec21 (ANR-11-LABX-0030) and of the PolyNat Carnot Institute (ANR-11-CARN-007-01). The authors thank Christine Lancelon-Pin (CERMAV-CNRS, Grenoble, France) for her assistance with scanning-electron microscopy. The authors acknowledge the NanoBio-ICMG chemistry platform (UAR 2607, Grenoble) for granting access to the electron microscopy facilities. We acknowledge the European Synchrotron Radiation Facility (ESRF) for providing beamtime.

References

Alting, A. C., Hamer, R. J., de Kruif, C. G., Paques, M., & Visschers, R. W. (2003). Number of thiol groups rather than the size of the aggregates determines the hardness of cold set whey protein gels. *Food Hydrocolloids*, *17*, 469–479.

Amagliani, L., van de Langerijt, T. M., Morgenegg, C., Bovetto, L., & Schmitt, C. (2023). Influence of charged and non-charged co-solutes on the heat-induced aggregation of soy and pea proteins at ph 7.0. *Food Hydrocolloids*, *137*, 108392.

Amagliani, L., & Schmitt, C. (2017). Globular plant protein aggregates for stabilization of food foams and emulsions. *Trends in Food Science & Technology*, *67*, 248–259.

Bonhomme, O., Morozov, A., Leng, J., & Colin, A. (2011). Elastic instability in stratified core annular flow. *Physical Review E*, *83*, 065301.

Cao, Y., & Mezzenga, R. (2019). Food protein amyloid fibrils: Origin, structure, formation, characterization, applications and health implications. *Advances in colloid and interface science*, *269*, 334–356.

Chen, N., Zhao, M., Chassenieux, C., & Nicolai, T. (2016). Thermal aggregation and gelation of soy globulin at neutral ph. *Food Hydrocolloids*, *61*, 740–746.

Cubaud, T., & Notaro, S. (2014). Regimes of miscible fluid thread formation in microfluidic focusing sections. *Physics of Fluids*, *26*, 122005.

Echaniz, C., de Loubens, C., Izeppi, D. M., & Chèvremont, W. (2025). (u)saxs measurement on protein aggregates [data set]. *European Synchrotron Radiation Facility*, *doi.org/10.15151/ESRF-ES-879022036*.

Fan, Y., Zeng, X., Yi, J., & Zhang, Y. (2020). Fabrication of pea protein nanoparticles with calcium-induced cross-linking for the stabilization and delivery of antioxidative resveratrol. *International journal of biological macromolecules*, *152*, 189–198.

Gimel, J. C., Durand, D., & Nicolai, T. (1994). Structure and distribution of aggregates formed after heat-induced denaturation of globular proteins. *Macromolecules*, *27*, 583–589.

de Guibert, D., Hennetier, M., Martin, F., Six, T., Gu, Y., Le Floch-Fouéré, C., Delaplace, G., & Jeantet, R. (2020). Flow process and heating conditions modulate the characteristics of whey protein aggregates. *Journal of Food Engineering*, *264*, 109675.

Kharlamova, A., Nicolai, T., & Chassenieux, C. (2018). Calcium-induced gelation of whey protein aggregates: Kinetics, structure and rheological properties. *Food Hydrocolloids*, *79*, 145–157.

Kouhi, M., Prabhakaran, M. P., & Ramakrishna, S. (2020). Edible polymers: An insight into its application in food, biomedicine and cosmetics. *Trends in Food Science & Technology*, *103*, 248–263.

Kumar, M., Tomar, M., Punia, S., Dhakane-Lad, J., Dhumal, S., Changan, S., Senapathy, M., Berwal, M. K., Sampathrajan, V., Sayed, A. A. et al. (2022). Plant-based proteins and their multifaceted industrial applications. *LWT*, *154*, 112620.

Li, T., Zhou, J., Peydayesh, M., Yao, Y., Bagnani, M., Kutzli, I., Chen, Z., Wang, L., & Mezzenga, R. (2023). Plant protein amyloid fibrils for multifunctional sustainable materials. *Advanced Sustainable Systems*, (p. 2200414).

Mehalebi, S., Nicolai, T., & Durand, D. (2008). Light scattering study of heat-denatured globular protein aggregates. *International Journal of Biological Macromolecules*, *43*, 129–135.

Moll, P., Salminen, H., Schmitt, C., & Weiss, J. (2021). Impact of microfluidization on colloidal properties of insoluble pea protein fractions. *European Food Research and Technology*, *247*, 545–554.

Moll, P., Salminen, H., Seitz, O., Schmitt, C., & Weiss, J. (2022). Characterization of soluble and insoluble fractions obtained from a commercial pea protein isolate. *Journal of Dispersion Science and Technology*, (pp. 1–12).

Narayanan, T., Sztucki, M., Van Vaerenbergh, P., Léonardon, J., Gorini, J., Claustre, L., Sever, F., Morse, J., & Boesecke, P. (2018). A multipurpose instrument for time-resolved ultra-small-angle and coherent X-ray scattering. *Journal of Applied Crystallography*, *51*, 1511–1524.

Schmitt, C., Bovetto, L., Buczkowski, J., Reis, G. D. O., Pibarot, P., Amagliani, L., & Dombrowski, J. (2021). Plant proteins and their colloidal state. *Current Opinion in Colloid & Interface Science*, *56*, 101510.

Silva, J. V., Balakrishnan, G., Schmitt, C., Chassenieux, C., & Nicolai, T. (2018). Heat-induced gelation of aqueous micellar casein suspensions as affected by globular protein addition. *Food Hydrocolloids*, *82*, 258–267.

Sim, S. Y. J., Srv, A., Chiang, J. H., & Henry, C. J. (2021). Plant proteins for future foods: A roadmap. *Foods*, *10*, 1967.

Tanger, C., Quintana Ramos, P., & Kulozik, U. (2021). Comparative assessment of thermal aggregation of whey, potato, and pea protein under shear stress for microparticulation. *ACS Food Science & Technology*, *1*, 975–985.

Vilotte, A., Bodiguel, H., Ako, K., Gunes, D. Z., Schmitt, C., & de Loubens, C. (2021). Kinetic and structural characterization of whey protein aggregation in a millifluidic continuous process. *Food Hydrocolloids*, *110*, 106137.

Vilotte, A., de Loubens, C., Gunes, D. Z., Schmitt, C., & Bodiguel, H. (2022). Hydrodynamic spinning of protein fractal aggregates into core–shell fibers. *ACS Applied Polymer Materials*, *4*, 4075–4080.